THE JOURNAL OF PHYSICAL CHEMISTRY C

Article

Cite This: J. Phys. Chem. C 2018, 122, 19481−19490

pubs.acs.org/JPCC

Adsorption of Acetone on Rutile TiO_2: A DFT and FTIRS Study

Tim Würger,[†,‡] Wolfgang Heckel,[†] Kai Sellschopp,[†] Stefan Müller,[†] Andreas Stierle,[§,∥] Yuemin Wang,[⊥] Heshmat Noei,[*,§] and Gregor Feldbauer[*,†]

[†]Institute of Advanced Ceramics, Hamburg University of Technology, D-21073 Hamburg, Germany

[‡]MagIC—Magnesium Innovation Centre, Helmholtz-Zentrum Geesthacht, D-21502 Geesthacht, Germany

[§]Deutsches Elektronen-Synchrotron (DESY), D-22607 Hamburg, Germany

[∥]Department Physik, Universität Hamburg, D-20355 Hamburg, Germany

[⊥]Institute of Functional Interfaces, Karlsruhe Institute of Technology, D-76131 Karlsruhe, Germany

Supporting Information

ABSTRACT: Acetone adsorbed on rutile TiO_2 nanoparticles was investigated with respect to its energetic, vibrational, and chemical properties. Temperature-dependent ultrahigh-vacuum Fourier transform infrared spectroscopy measurements for different acetone dosages (4.5−900 L) give insights into the acetone adsorption behavior. Those experiments indicate thermal-induced reactions of acetone on rutile TiO_2 surfaces yielding new species. Density functional theory calculations were performed to investigate acetone adsorption on rutile TiO_2(110). Particularly, the importance of sampling the adsorption configuration space is shown. Adsorption geometries that are energetically significantly more favorable than the commonly used high-symmetry configurations are presented. To facilitate the comparability to the experiment, theoretical infrared spectra were computed using density functional perturbation theory for various acetone adsorption geometries using different exchange-correlation functionals. Additionally, computational spectra were obtained for several species which are potential products from reactions of acetone on TiO_2 surfaces. The investigated species are η^2-acetate, η^2-diolate, η^1-enolate, and mesityl oxide. For η^1-acetone, experimental and calculated spectra fit well for low temperatures, whereas for elevated temperatures, emerging bands indicate the formation of diolate.

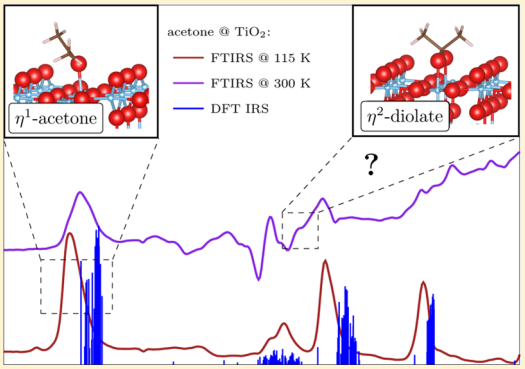

INTRODUCTION

The adsorption and possible subsequent chemical decomposition of acetone on titania (TiO_2) surfaces are of broad interest because of their relevance in various processes ranging from photocatalysis[1−6] to the remediation of airborne acetone contaminants.[1,7] At hybrid interfaces between inorganic surfaces and organic linker molecules, acetone may act as a competitor to coupling agents like carboxylic acids.[8−10] Thus, a detailed understanding of the relevant adsorption phenomena is crucial. In general, acetone is present in numerous chemical processes because of its usage as solvent or reagent.[11] Particularly, acetone often occurs in catalytic reactions as a reactant, intermediate, or product. On oxidized TiO_2 surfaces, acetone is photochemically active[12] and associated phenomena have raised widespread interest.[1,4]

Numerous studies of the acetone adsorption on TiO_2 exist, e.g., on the site competition during co-adsorption of acetone and other adsorbates,[7,12] on acetone-assisted oxygen vacancy diffusion,[13] as well as on its photochemistry.[1,2,4,5,14,15] In this regard, the well-studied (110) surface of rutile TiO_2 (r-TiO_2) serves often as an ideal single-crystal model system for surface-science studies.[16]

The adsorption of acetone on stoichiometric, oxidized, or reduced rutile TiO_2(110) surfaces was investigated previously by different groups.[12,17−19] In an experimental study, Henderson[19] presented six different species potentially occurring upon the interaction of acetone with a rutile TiO_2(110) surface. At low temperatures and at a clean surface, acetone is supposed to adsorb as η^1-acetone.[6,20] Since this species dominates at low temperatures and high coverages, it is the main subject of the computational part of this study. Other species only seem to emerge under specific conditions.[6,20] In the presence of adsorbed oxygen, such conditions are, for example, elevated temperatures for η^2-diolate formation[1] and UV irradiation for obtaining η^2-acetate from diolate and η^1-enolate directly from acetone.[15]

In a computational study, Márquez et al.[21] examined the adsorption of acetone on rutile TiO_2(110) with respect to the influence of adsorption site, coverage, and geometry. They observed a strong dependence of the binding energy on these

Received: May 3, 2018
Revised: July 18, 2018
Published: August 20, 2018

DOI: 10.1021/acs.jpcc.8b04222
J. Phys. Chem. C 2018, 122, 19481−19490

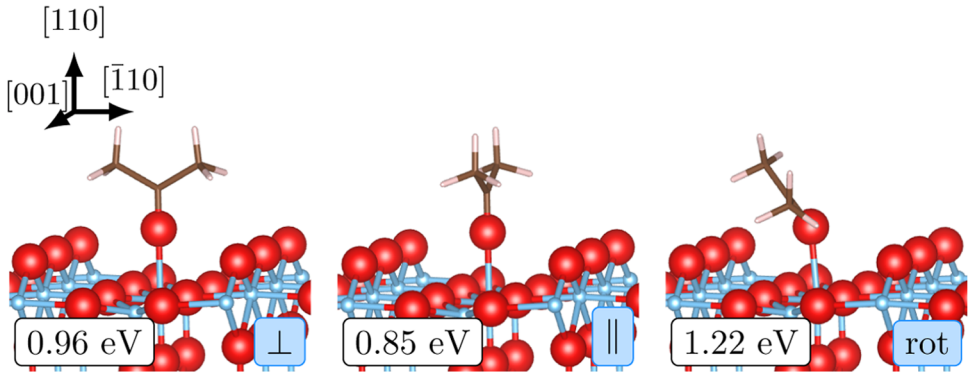

Figure 1. Calculated relaxed η^1-acetone structures on rutile TiO_2(110). The structures are categorized by the orientation of the molecular symmetry plane of the adsorbed acetone molecule relative to the row of bridging oxygen atoms. From left to right, the ⊥, ∥, and rot_{max} geometries are shown. The respective binding energies E_B (eV) are presented in white boxes. Color code: Ti = blue, O = red, C = brown, and H = whitish.

subjects. The binding energy of acetone is affected strongly by the coverage because of significant intermolecular repulsion at high coverages. The fivefold-coordinated titanium atoms produce a surface electric field, which is able to interact with an acetone molecule via the dipole of its carbonyl group. This interaction makes the adsorption of acetone favorable and advocates for two major adsorption sites. Acetone molecules are supposed to adsorb either on top of the fivefold-coordinated titanium atoms or in a bridging position between two of those titanium atoms. For each position, the $C(CH_3)_2$ complex can rotate around the C−O axis in a way that the acetone symmetry plane is perpendicular (⊥) to the row of bridging oxygen atoms, parallel (∥), or in between (rot) (see Figure 1).

In this study, we use ultrahigh-vacuum Fourier transform infrared spectroscopy (UHV-FTIRS) to investigate the adsorption and reactions of acetone on the surface of rutile TiO_2 nanoparticles. Such samples are considered more realistic model systems for catalysts than single-crystal surfaces. The IR results allow to identify species formed upon the interaction between acetone and TiO_2. The interpretation of the experimental results is assisted by theoretical IR spectra calculated within the framework of density functional theory (DFT). Polycrystalline rutile TiO_2 nanoparticles expose predominantly the (110) facet,[22] which is the most stable surface of rutile.[16] Therefore, this surface is investigated in the computational part of this work. The computational results are first validated with respect to published experimental work on single-crystal rutile TiO_2(110) surfaces, which are mentioned above. In a second step, the calculated results are compared to our experimental results on rutile TiO_2 nanoparticles to see if this allows for new insights. In the literature, the main focus of computational studies was put so far on ⊥- and ∥-adsorption orientations of acetone on rutile TiO_2(110); however, experimental results by Petrik et al. indicated a preference for tilted adsorption geometries for selected coverages.[1] For more details, the configuration space was sampled more exhaustively in this study by investigating numerous additional geometries computationally.

METHODS

Experimental Methods. For the UHV-FTIR measurements, the polycrystalline rutile TiO_2 (r-TiO_2) powder samples (100 $m^2\ g^{-1}$, Sachtleben) were first pressed onto a gold-plated stainless steel grid (0.5 × 0.5 cm^2) and then mounted on a sample holder to record FTIR data in transmission mode. The FTIR measurements on TiO_2 powder samples are done with an UHV apparatus, which combines a state-of-the-art vacuum IR spectrometer (VERTEX 80v, Bruker) with an UHV system.[23] The sample holders, on which the TiO_2 powder samples are mounted after they have been pressed, are specially designed for the FTIR transmission measurements under UHV conditions, allowing a rapid heating and cooling of the samples between 100 and 1000 K. The base pressure in the measurement chamber was 2 × 10^{-10} mbar. To achieve a high sensitivity and stability of the measurements, the adsorption of atmospheric moisture was prevented by evacuating the optical path inside the IR spectrometer and the space between the spectrometer and the UHV chamber. By heating to 750 K, the grid and the attached powder particles were cleaned in the UHV chamber to remove all contamination, such as water and hydroxyl groups. After annealing, no significant reduction of the sample was observed. Prior to each exposure to acetone, a spectrum of the clean TiO_2 powder was recorded as a background reference. All UHV-FTIR spectra were collected with 1024 scans at a resolution of 2 cm^{-1} in the transmission mode. Exposure of the sample to acetone was carried out by back-filling the measurement chamber through a leak valve.

Computational Methods. For a more comprehensive understanding of the adsorption behavior of acetone on a rutile TiO_2(110) surface, density functional theory (DFT) calculations were performed using the plane-wave code Vienna Ab Initio Simulation Package (VASP)[24−27] with the projector augmented wave (PAW) method.[28,29] Since van der Waals (vdW) interactions can be significant in the adsorption of organic molecules,[9] the exchange-correlation (XC) functional optB88-vdW[30−33] was used for all DFT calculations in this work. This functional belongs to the group of van der Waals density functionals (vdW-DF), based on an approach by Dion et al.[34] Within this approach, vdW interactions are accounted for without the use of external input parameters. Some approximations are, however, done such as that the vdW interactions are considered to be pairwise additive. Klimeš et al. introduced several vdW-DFs, the "opt" functionals,[30,31] which have been successfully applied to various systems.[35−41] In particular, the optB88-vdW functional is considered to capture well the subtle contributions of weak interactions in the adsorption of organic molecules.[42−44] For comparisons and consistency checks, the main results were reproduced using various other XC functionals, namely, PBE,[45] PBEsol,[46] and PW91[47] (see the Supporting Information).

DOI: 10.1021/acs.jpcc.8b04222
J. Phys. Chem. C 2018, 122, 19481−19490

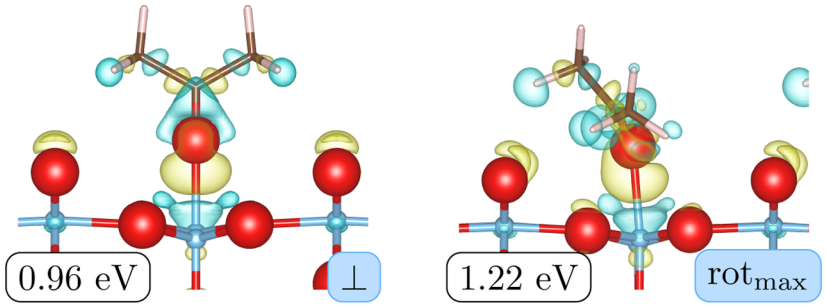

Figure 2. Illustration of the calculated adsorption-induced changes in the electronic charge distributions for acetone molecules adsorbed in the ⊥- and rot$_{max}$-orientations on rutile TiO_2(110). Color code: yellow and blue represent excess and deficiency of electrons, respectively.

All calculations were performed using a 5 × 5 × 1 Monkhorst−Pack set of *k*-points.[48] The plane-wave expansion was limited by a cutoff energy of 520 eV. During the relaxation process, the atom positions were allowed to adjust until the atomic forces were less than 5 meV Å^{-1}. For the relaxation process, the systems were preconverged using the conjugate gradient algorithm and then a quasi-Newton algorithm was employed, which is efficient close to a minimum. Finally, the structure was investigated statically to obtain more accurate total energies via the tetrahedron method with Blöchl corrections.[49]

The surface was modeled using a slab of five O−Ti−O layers in a 2 × 1 surface cell. Atoms in the two lowermost layers were kept fixed in their bulklike positions, whereas the remaining layers were free to relax, thus being able to respond to occurring forces due to surface effects or adsorption. A vacuum region of 23 Å was added above the slab to avoid interaction between the periodic images.[50] A dipole correction is applied to compensate for the slab asymmetry.[51,52] Binding energies E_B of adsorbed acetone on rutile TiO_2(110) were determined as the difference between total energies of the educts, $nE_{adsorbate,gas}$ and $E_{substrate}$, and the total energy of the product, $E_{subs+ads}$, divided by the number of adsorbed molecules per cell *n*

$$E_B = \frac{1}{n}(nE_{adsorbate,gas} + E_{substrate} - E_{subs+ads}) \quad (1)$$

To find the ground state of adsorbed acetone on rutile TiO_2(110), it is not sufficient to investigate a randomly oriented molecule. Large energy barriers and large distances prevent atom movement to the ground-state position during relaxation due to the respective algorithm design in DFT codes. A starting position of the molecule close to the ground state is therefore crucial. To this end, an in-house MATLAB code was used to generate a solution space of distinct acetone molecule geometries on the surface slab. The code includes coarse graining and symmetry check algorithms to minimize the number of initial configurations.

In addition to the total energy calculations, vibrational spectra were analyzed using density functional perturbation theory (DFPT).[53,54] In DFPT, the vibrational frequencies in the harmonic approximation are obtained via the dynamical matrix, which is calculated by slightly displacing selected atoms from their ground-state positions and recording the resulting electron density response. Here, the atoms of the adsorbed acetone molecule and the adsorption site Ti atom are allowed to be displaced. Furthermore, it is possible to compute the matrix of Born effective charges (BECs), which refers to the change of an atom's polarization when exposed to an external electric field. Using the formula by Gianozzi and Baroni[55,56] and the procedure proposed by Karhánek et al.,[57] the BEC matrix leads to the oscillator strengths, or rather vibrational intensities. Combined with the vibrational frequencies from the dynamical matrix, the infrared (IR) spectra for acetone in the gas phase and for adsorbed species can be calculated. It has to be noted that following this DFT-based method, the calculated vibrational frequencies typically deviate from experimental results by a few percents.[58−60] The vibrational frequencies tend to be underestimated for generalized gradient approximation (GGA)(-based) functionals. The error occurs mainly because of the harmonic and density functional approximation, which, however, partially compensates for GGA(-based) functionals.[61,62]

RESULTS AND DISCUSSION

Geometries. As mentioned in Introduction, acetone can adsorb on a rutile TiO_2(110) surface in various geometries. Since the main focus in earlier computational studies[21] was put on high-symmetry geometries, in this study, the configuration space was sampled more exhaustively by generating around 50 η^1-acetone input structures. These structures were set up with an in-house MATLAB code to cover a high number of distinct orientations. In the following, adsorbed molecules are classified according to the orientation of their molecular symmetry plane with respect to the rows of bridging oxygen atoms of a rutile TiO_2(110) surface. Except for the geometries with perpendicular (⊥) or parallel (∥) molecular and bridging oxygen planes, all other structures are labeled as rot-geometries. In each 2 × 1 surface supercell, one molecule was placed, resulting in a total coverage of θ = 0.5 monolayer (ML). Deviating coverages are clearly indicated in the following.

In Figure 1, relaxed η^1-acetone geometries, including their respective calculated binding energies E_B, are shown. In addition to the ⊥- and ∥-orientated η^1-acetone molecules, also an energetically more favorable rot-orientation is presented. This rot-geometry exhibits the largest binding energy found in this study and will be referred to as rot$_{max}$. The computed binding energies range from 0.85 to 1.22 eV when using the optB88-vdW XC functional. A preference for rot-orientations is in agreement with experimental indications in the literature.[1] For comparison and consistency, binding energies using other XC functionals were determined for the main geometries (see the Supporting Information). Even though the binding energies depend sensitively on the employed XC functional, the energetic tendencies and relations between the different geometries remain the same. Since the optB88-vdW functional is expected to adequately represent the energetic impact of the adsorbed molecule,[9] it is used for further computations.

DOI: 10.1021/acs.jpcc.8b04222
J. Phys. Chem. C 2018, 122, 19481−19490

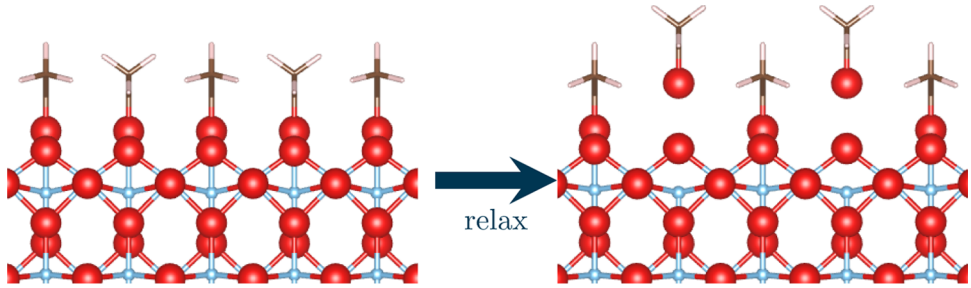

Figure 3. Formation of a bilayer of acetone on rutile $TiO_2(110)$ upon calculated ionic relaxations starting from a ⊥ adsorption configuration with a coverage of θ = 1 ML. Color code: Ti = blue, O = red, C = brown, and H = whitish.

Enhanced and more directional interactions of the methyl groups with neighboring bridging oxygen atoms are found for the rot_{max} geometry comparing the differences of electron charge densities for the ⊥ and rot_{max} geometries (see Figure 2). This gives an indication why rot-geometries are favorable in terms of the binding energy. Such differences are obtained by subtracting the charge densities of the isolated molecule and surface from the charge density of the adsorption configuration.

So far, all investigated surface slabs had a coverage of θ = 0.5 ML. However, in a 2 × 1 surface slab, there are two fivefold-coordinated titanium atoms and thus two possible acetone adsorption sites. To investigate the full coverage (θ = 1 ML) of the rutile $TiO_2(110)$ surface, two acetone molecules in ⊥-orientation were placed manually on the surface. Due to the steric hindering of neighboring periodic molecules, only ⊥-orientations similar to Figure 1 (left) can lead to high coverages. During the relaxation, however, the distance between the acetone molecules in every second row in the [001] direction and the surface is increased and a second layer of adsorbed molecules is formed as illustrated in Figure 3. This structure is referred to as bilayer in the following. The total binding energy of the bilayer amounts to about 1.3 eV per 2 × 1 surface cell. The relaxed adsorption geometry of acetone molecules close to the surface within the bilayer is almost identical to the ⊥ configuration at θ = 0.5 ML. Consequently, we assume that these acetone molecules are bound to the surface with a similar strength as the ⊥ configuration at 0.5 ML. Comparing the total binding energies, the molecules of the bilayer further away from the surface are associated with only a small binding energy of about 0.34 eV per molecule. Thus, within the bilayer, the second layer binds much weaker than the first layer.

In Table 1, the binding energies per molecule are presented for different acetone coverages on the rutile TiO_2 surface. Here, binding energies for coverages of 1 and 0.5 ML are determined using 2 × 1 supercells, while for a coverage of 0.125 ML, a 4 × 2 supercell was employed. Results show an increase in binding energy per molecule as the coverage decreases. For a coverage of 1 ML, only the ⊥-configuration of adsorbed acetone is possible for geometrical reasons and the average binding energy per molecule amounts to 0.65 eV. For coverages of 0.5 and 0.125 ML, the rot_{max}-configuration remains the energetically most favorable adsorption structure with binding energies per molecule of 1.22 and 1.38 eV, respectively. The variation in the binding energies of the studied configurations is significantly smaller for 0.125 ML than for 0.5 ML. The coverage dependence of the adsorption energy is in qualitative agreement with temperature-programmed desorption experiments in the literature.[19] In that work also, low-temperature desorption peaks occurred for coverages above 0.5 ML, indicating more weakly bound acetone molecules. Although experiments suggest tilted adsorption geometries for coverages of 0.33 and 0.6 ML, for 0.17 ML, a ⊥-configuration is indicated.[1] The latter is not in agreement with our computational results, although we also observe a less pronounced preference for rot-configurations at low coverage. Since, however, the focus of the cited experimental work was not on the orientation, a more dedicated single-crystal study should be performed on this subject in future. Petrik et al.[1] assumed that intermolecular repulsion at increased coverages favors tilted configurations. The decreasing binding energy with increasing coverage (see Table 1) also points toward that explanation. For further clarification, we calculated total energies for acetone molecules in different adsorption geometries (see Figure 1) in the same simulation cell as the previous calculations, however, without the TiO_2 slab. Comparing these results for different geometries and to corresponding calculations including the TiO_2 slab shows an additional stabilization of the rot-geometry with respect to the ⊥-orientation because of interactions with the slab. Such contributions have already been indicated above by the changes in the charge densities (see Figure 2).

Table 1. Calculated Binding Energies per Acetone Molecule on a Rutile $TiO_2(110)$ Surface for Different Coverages θ (in ML)[a]

	binding energy/molecule (eV)		
configuration	1 ML	0.5 ML	0.125 ML
∥		0.85	1.18
⊥	0.65	0.96	1.22
rot_{max}		1.22	1.38

[a]For 1 ML, only the ⊥-configuration of adsorbed acetone is possible.

The formation of new species upon acetone adsorption and potential temperature-activated reactions can be monitored by UHV-FTIRS performed at different temperatures. To provide a theoretical reference for species determination, DFPT is used to compute the vibrational spectra of several species that are likely products of reactions of acetone on $TiO_2(110)$, including η^2-acetate, η^2-diolate, η^1-enolate, and mesityl oxide.[19] Relaxed structures of these species are illustrated in Figure 4.

Energy−Geometry Relationship. With regard to the acetone geometries in Figure 1, the relationship between adsorption structure and respective binding energies is not obvious. Despite the fact that the difference of 0.1 eV between the ⊥-orientation (Figure 1, left) and ∥-orientation (Figure 1, middle) corresponds to the literature,[21] rot-orientations reach even higher binding energies. Since also other adsorption

DOI: 10.1021/acs.jpcc.8b04222
J. Phys. Chem. C 2018, 122, 19481−19490

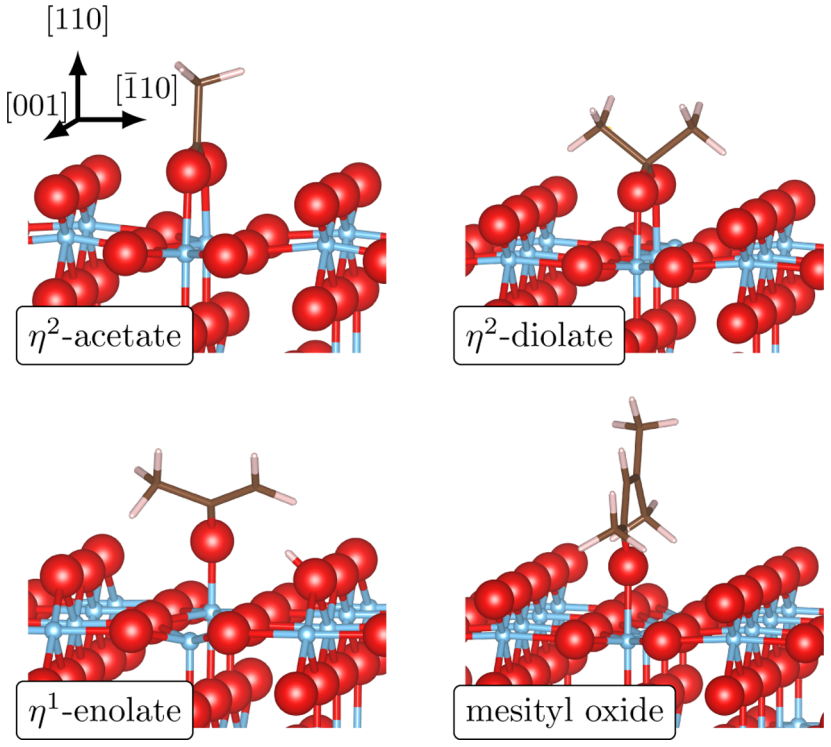

Figure 4. Illustration of potential reaction products of acetone adsorbed on TiO_2, including η^2-acetate, η^2-diolate, η^1-enolate, and mesityl oxide. Color code: Ti = blue, O = red, C = brown, and H = whitish.

angles seem to have an influence on the energetics, two adsorption angles, φ and ϑ, are defined and investigated with respect to their effect on the binding energies. For η^1-enolate on rutile TiO_2(110), a similar study is presented in the Supporting Information

Due to possible hydrogen bonds, the positions of the two methyl groups within the acetone molecule have a large impact on the energetics of the adsorption. First, these positions are further specified using the adsorption angles φ and ϑ. In Figure 5, the locations of the carbon atoms are used to define a plane that is parallel to the symmetry plane of the molecule. Additionally, the surface normal of the (110)-plane serves as a reference. Considering possible interactions of the methyl groups with surface atoms, particularly the bridging oxygen atoms, the angle ϑ between the $C_1-C_2-C_3$ plane and surface normal is of high interest. To facilitate the comparison to the literature, $\vartheta = 0°$ corresponds to an upright position of the acetone molecule. The angle describing the ⊥-, rot-, and ∥-orientations of the acetone symmetry plane in relation to the row of bridging oxygen atoms is defined as φ. To this end, the vector between the methyl-group carbon atoms C_2 and C_3 as well as the vector between adjacent bridging oxygen atoms are projected into the (110)-plane. Investigating the influence of φ on the binding energy can also give information about possible methyl-group interaction with the surface atoms. Additionally, it is possible to define two angles between the oxygen atom of the carbonyl group, the adjacent carbon atom C_1, and the respective carbon atoms C_2 and C_3 of the methyl groups. Considering these two angles, the tilt around the linking carbon atom C_1 in the $C_1-C_2-C_3$ plane can be described. However, investigating all η^1-acetone adsorption structures for these two angles showed only slight deviations from the symmetric state. After relaxation of the input structures with tilting angles between 0 and 6°, the majority of acetone geometries converged with a tilting angle of around 2°, showing an angle preference of the carbon orbitals.

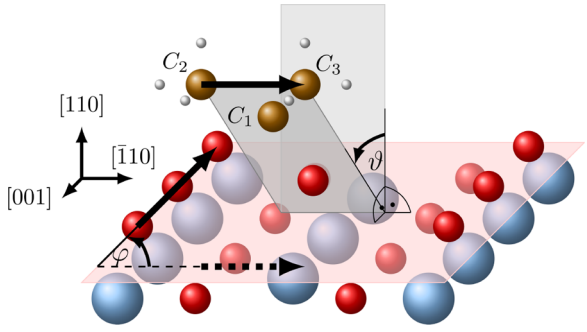

Figure 5. Sketch showing the binding angles φ and ϑ. The angle φ describes the rotation of the methyl groups with respect to the rows of bridging oxygen atoms, where $\varphi = 0°$ corresponds to a ∥-orientation and $\varphi = 90°$ corresponds to a ⊥-orientation. The angle ϑ describes the inclination of the plane spanned by the three carbon atoms with respect to the surface normal. Color code: Ti = blue, O = red, C = brown, and H = whitish.

All energy−angle relations of adsorbed η^1-acetone are presented in Figure 6. For an angle φ roughly between 20 and 65° (rot-orientation), the highest binding energies (>1.2 eV) were determined, while between 38 and 50° also lower energies of around 1.05 eV occur. Approaching the ⊥- or ∥-orientation, the binding energies continue to decline, yielding the minima for the ⊥-orientation and ∥-orientation at 0.96 and 0.85 eV, respectively. However, for two cases with a ∥-like orientation ($\varphi < 10°$), the binding energies are also higher than 1.2 eV. For angles ϑ between 20 and 50°, or rather for a shorter distance of the methyl groups to the surface, the resulting binding energies are higher as well (slightly above 1.1

DOI: 10.1021/acs.jpcc.8b04222
J. Phys. Chem. C 2018, 122, 19481−19490

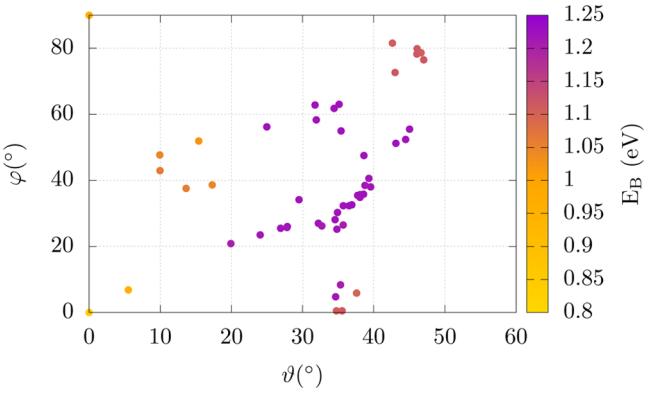

Figure 6. Calculated binding energies with respect to the adsorption angles φ and ϑ (see Figure 5) for all relaxed adsorption geometries of acetone on rutile TiO_2(110) considered in this study. The color code gives the corresponding binding energies E_B (eV).

or 1.2 eV). For completely upright positions ($\vartheta = 0°$), the same minima as for $\varphi = 0$ and 90° can be seen. By investigating both angles at the same time a lumped area of high binding energies at $30° < \vartheta < 50°$ and $20° < \varphi < 60°$ can be seen, marking an area of energetically favorable and distinct η^1-acetone geometries.

Because of the small energy differences between many adsorption geometries, it is expected that numerous configurations in the energetic vicinity of the most favorable one are realized at finite temperatures. Furthermore, continuous transitions between different geometries may occur.

UHV-FTIRS Results. Figure 7 shows the experimental IR spectra recorded for acetone adsorption on the pure, adsorbate-free rutile TiO_2 powder sample at 115 K. After exposure to acetone, a number of IR bands are observed at 2909, 1711, 1695, 1440, 1420, 1363, and 1229 cm^{-1}, which are related to the adsorption of acetone on the rutile TiO_2 surface. Polycrystalline rutile TiO_2 nanoparticles expose predominantly the (110) facet,[22] which is the most stable surface of rutile.[16] The obtained IR bands fit well to those reported for single-crystal rutile TiO_2(110) surfaces.[1]

To get deeper insight into the adsorption of acetone on rutile TiO_2(110), we have carried out temperature-dependent IR measurements. The sample was heated up to elevated temperatures after acetone adsorption at 115 K. The obtained IR spectra are displayed in Figure 8. After annealing the sample to 150 K, most IR bands decreased only slightly in intensity, revealing the chemisorption of acetone molecules on TiO_2(110). On the basis of the literature, the dominating IR bands at 2909, 1711, 1420, 1363, and 1229 cm^{-1} are attributed to the ν(C−H), ν(C═O), $\sigma_{as}(CH_3)$, $\sigma_s(CH_3)$, and ν(C−C) vibrations of acetone,[6,15] respectively. Although it is possible to get a multilayer of acetone on TiO_2 surfaces at 115 K, the IR spectra do not show characteristic bands for multilayer adsorption. This can be explained with the high surface area of the powder samples, which need a much higher amount of acetone for covering the whole surface. Annealing the sample up to 150 K leads to a partial removal of acetone, verified by a decrease of the asymmetry and symmetry vibrational bands of CH_3, $\sigma_{as}(CH_3)$, and $\sigma_s(CH_3)$ at 1420 and 1363 cm^{-1}, while new vibrational bands appeared at 2974, 1695, 1498, 1434, and 1170 cm^{-1} and grew in intensity with increasing temperature. Simultaneously, the intensity of molecular acetone-related IR vibrations declined significantly at higher temperatures. These findings (see Figure 8) indicate thermal-induced reactions of acetone on rutile TiO_2 surfaces yielding new species. The 1434 cm^{-1} band is characteristic for the symmetry mode of O−C−O stretching vibrations, which is formed on the surface when acetone interacts with surface oxygen. The corresponding ν_{as}(OCO) vibration was observed at 1498 cm^{-1}. At 250 K, the ν(C═O) band splits into two peaks (zoom in Figure 8) centered at 1711 and 1695 cm^{-1}.

Computational Vibrational Analysis. The wavenumbers of the most relevant vibrational modes of acetone are presented in Table 2. Experimental as well as calculated values are given for adsorbed and gas-phase acetone molecules. The computational results for adsorbed acetone are given for the rot_{max} configuration with the largest binding energy (see Figure 1). An isolated acetone molecule is also analyzed computationally to simulate the gas phase before adsorption. Additionally, experimental results for the gas phase and for acetone adsorbed on rutile TiO_2(110) from the literature[1,63] are presented to show the accuracy and validity of the chosen method. The computed wavenumbers agree very well with the experimental values.

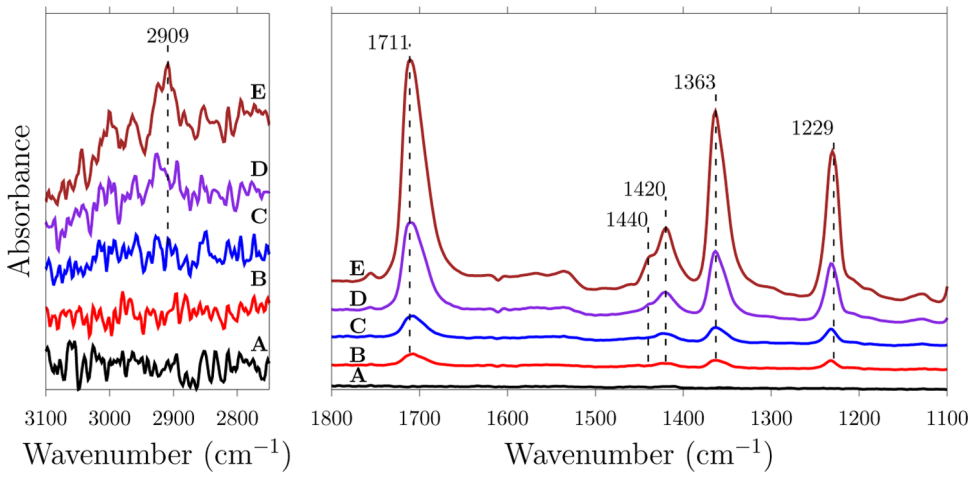

Figure 7. Experimental UHV-FTIR spectra obtained after exposing the clean rutile TiO_2 powder to different doses of acetone at 115 K in an UHV chamber. The sample was prepared via heating in the UHV chamber to 750 K to remove all adsorbed species; (A) clean surface and (B−E) exposure to acetone: (B) 4.5 L, (C) 45 L, (D) 375 L, and (E) 900 L.

DOI: 10.1021/acs.jpcc.8b04222
J. Phys. Chem. C 2018, 122, 19481−19490

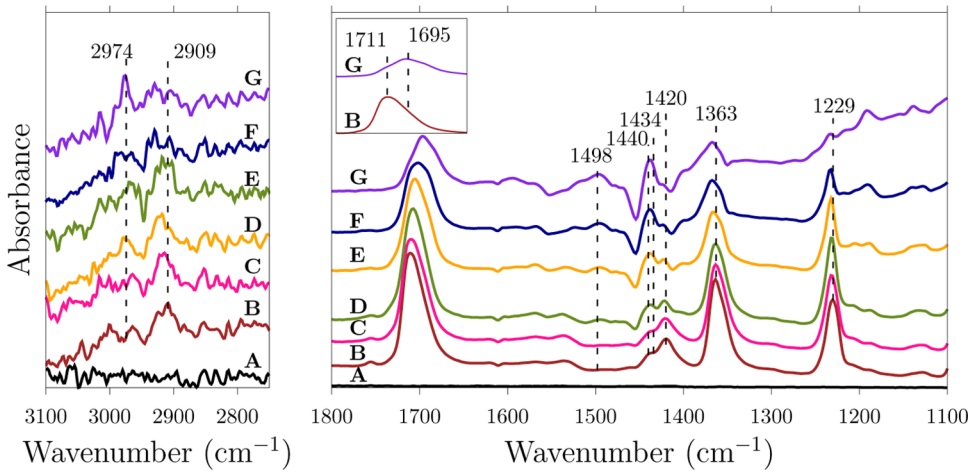

Figure 8. Experimental UHV-FTIR spectra obtained after exposing the clean rutile TiO_2 powder to different doses of acetone in a UHV chamber and annealing at elevated temperatures. (A) Clean surface, (B) exposure to 900 L acetone at 115 K, and annealing at (C) 120 K, (D) 150 K, (E) 200 K, (F) 250 K, and (G) 300 K.

Table 2. Measured, within Current Work (Exp) as Well as from the Literature (Lit), and Calculated (Calc) Vibrational Frequencies for Acetone in the Gas Phase and Adsorbed η^1-Acetone on Rutile TiO_2[a]

	wavenumber (cm^{-1})				
band	gas$_{lit}$ [63]	gas$_{calc}$	adsorbed$_{exp}$	adsorbed$_{calc}$	adsorbed$_{lit}$ [1]
ν(C−C)	1216	1210	1229	1217	1232
σ_s(CH$_3$)	1364	1346	1363	1335	1372
σ_{as}(CH$_3$)	1435	1425	1420	1409	1422
ν(C═O)	1731	1731	1711	1671	1705
ν(C−H)	2937	2957	2909	2897	

[a]The computational and literature values for adsorbed acetone were obtained at the (110) surface for the calculated ones in the rot$_{max}$ configuration (see Figure 1).

The adsorption of the acetone molecule is indicated by peak shifts to lower frequencies of the C═O bonds. Generally, peak shifts to lower frequencies can also occur because of interactions with heavier atoms. Hence, the peak shift to 2897 cm^{-1} of the C−H stretching bond in η^1-acetone might indicate hydrogen bonds, explaining the higher binding energy of 1.22 eV in the rot-geometry.

To check the consistency of the employed computational method, the vibrational analysis was performed using various XC functionals. Details can be found in the Supporting Information. Summarizing, the results for C−C and C═O modes differ within a range of less than 2% for the tested functionals. For modes including hydrogen, the range shifts up to about 3%. A comparison with the experimental results (see Table 2) shows that the values deviate within about 2%. Although no functional can be considered genuinely superior to the others regarding this vibrational analysis, optB88-vdW yields the smallest average deviations from experimental results. For optB88-vdW, all bands are shifted to lower wavenumbers with respect to the experiment.

Considering the small energy differences between various adsorption geometries, it has to be expected that numerous configurations occur at finite temperatures. Consequently, various geometries contribute to a measured IR spectrum.

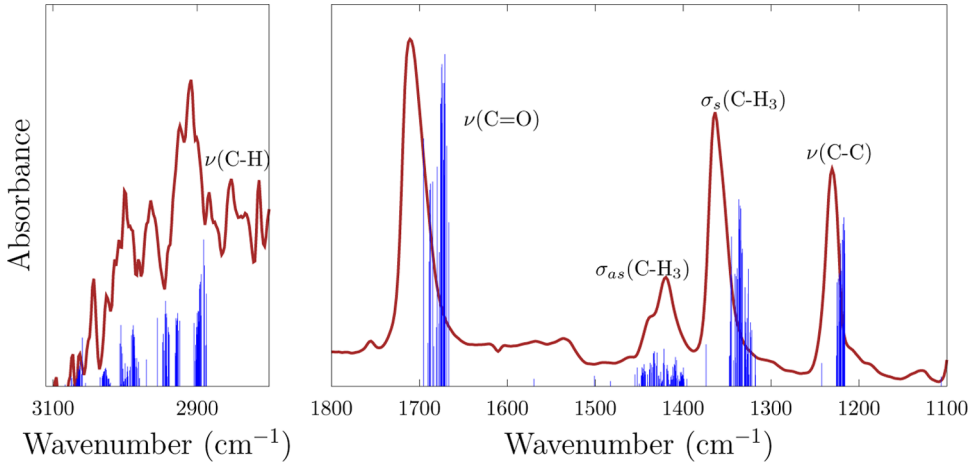

Figure 9. Calculated (blue) and experimental (brown) infrared spectra of η^1-acetone adsorbed on rutile TiO_2(110). The theoretical spectrum is a superposition of the spectra for all calculated configurations exhibiting binding energies within 30 meV to the most favorable rot$_{max}$ geometry (see Figures 1 and 6). The contributions of the different configurations are weighted using a Boltzmann factor according to their differences in binding energy and a temperature of 115 K.

DOI: 10.1021/acs.jpcc.8b04222
J. Phys. Chem. C 2018, 122, 19481−19490

Since the vibrational features depend on the specific configuration, the resulting spectrum will be broadened. Figure 9 shows a comparison between a measured IR spectrum (see Figure 7, curve E) and a calculated spectrum including all investigated adsorption geometries yielding binding energies within 30 meV of the most favorable structure. The calculated spectrum of each structure is first normalized to its highest peak. Then, for a temperature of T = 115 K, following the experimental setup, a Boltzmann factor ($\exp(-\Delta E/k_B T)$) with the Boltzmann constant k_B is used to scale the computed IR peaks for each structure using the energy difference ΔE associated to the most favorable structure. The computed vibrations are in good agreement with the experimental results. In particular, positions and hierarchy of intensities of the ν(C═O), σ_s(C−H_3), and ν(C−C) bands correspond well to the UHV-FTIR measurements in the literature on single-crystal rutile TiO_2(110) surfaces[1] as well as to our experimental results on rutile TiO_2 nanoparticles. As expected, the calculated IR bands are slightly shifted toward lower wavenumbers (see Computational Methods). Because of the agreement to various experiments, we believe that we can use our DFT results to learn more about the adsorption on the nanoparticles as well, even though we are missing contributions from minority surface orientations and from features such as edges and kinks.

The vibrational properties of further compounds that may occur upon temperature- or UV-light-induced chemical reactions of the adsorbed acetone molecules[19] were calculated. The possibly relevant compounds are η^2-acetate, η^2-diolate, η^1-enolate, and mesityl oxide. Along with the experimental UHV-FTIR spectra recorded at elevated temperatures (see Figure 8), the calculated vibrational spectra for all relevant species are presented in Figure 10.

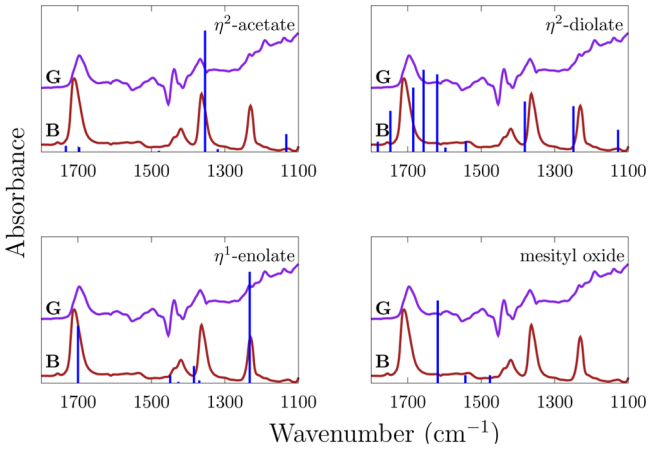

Figure 10. Comparison of calculated vibrational spectra (blue lines) of four species adsorbed on rutile TiO_2(110) (see Figure 4) and the experimentally recorded FTIR spectra at 115 K (B) and 300 K (G), as presented in Figure 8.

The temperature-induced shifts in the experimental FTIR spectra clearly indicate modifications of the adsorbed acetone molecules. Even though some bands of the calculated IR spectra for η^2-acetate, η^1-enolate, and mesityl oxide seem to match areas of the recorded FTIR spectra, they do not account for the major temperature-induced changes of the experimental spectra. In more detail, acetate and enolate share some major IR peaks with acetone because of common vibrational modes. Both species, however, do not exhibit IR bands that can explain the emerging IR features upon increasing temperature during the experiments. For mesityl oxide, no major agreement between the calculated IR spectra and any experimental one is observed. This allows to rule out the formation of significant amounts of mesityl oxide under specific experimental conditions. Moreover, the formation of large amounts of the three species is rather unlikely considering the experimental conditions.[1,15,19,20] The observed splitting of the ν(C═O) band at a temperature of 250 K (1711 and 1695 cm^{-1}) fits well to the calculated spectrum of diolate with multiple bands in the same region. Furthermore, bands at 1381 and 1128 cm^{-1} match peaks in the spectrum for 300 K (G). Since only the major surface orientation, no defects, and only a few adsorption geometries of the possibly relevant compounds were investigated, lacking bands at certain frequencies are expected. Additionally, interactions between acetone and the new species, which could affect the IR spectra, are not investigated. Similar to results from the literature,[1] the formation of a significant amount of diolate seems to be plausible considering the observed IR spectra at the investigated temperatures. The work by Petrik et al.[1] was done on reduced and oxidized surfaces. Diolate formation was shown there for oxidized samples. However, in their IR data, diolate bands seem to appear for high acetone coverages on reduced samples, too. Our current results indicate that diolate also forms at high coverages for neither significantly reduced nor oxidized surfaces. Furthermore, defects such as steps, edges, and kinks, which are more common for nanoparticles, could affect the results as well as adsorption from the residual gas. Thus, subsequent detailed studies should be performed in the future to shed further light on these issues.

CONCLUSIONS

In this study, the adsorption behavior of acetone on rutile TiO_2 was investigated with respect to its energetic, vibrational, and chemical properties. A joint approach combining experimental and theoretical techniques was chosen allowing for a detailed analysis of the investigated system. Using UHV-FTIR measurements at 115 K for different acetone dosages (4.5−900 L) and annealing at various temperatures (120−300 K), insights into the acetone adsorption behavior could be obtained, where the formation of new species with increasing temperatures was indicated by modified IR spectra. Additionally, an extensive DFT study of numerous acetone adsorption geometries and coverages improved the understanding of acetone adsorption on the rutile TiO_2(110) surface. Complementing previous work in the literature, here the configuration space was sampled more exhaustively. Investigating the binding angles of acetone molecules with respect to the corresponding binding energy indicates a large number of adsorption geometries energetically close to the most favorable calculated configuration. Those geometries exhibit rotated and tilted molecular symmetry planes with respect to the surface features, while highly symmetrically adsorbed acetone molecules correspond to significantly lower binding energies. Considering the small energy differences between various adsorption geometries, continuous transitions between structures may occur. Using DFPT, computed IR spectra for the investigated acetone adsorption geometries as well as for potential acetone reaction products were used to complement the experimental FTIRS results. At low temperatures, the theoretical and experimental IR spectra are in good agreement

DOI: 10.1021/acs.jpcc.8b04222
J. Phys. Chem. C 2018, 122, 19481−19490

with each other and with results from the literature on single-crystal rutile TiO_2(110) surfaces. IR bands computed with DFPT are generally shifted toward lower wavenumbers. For higher temperatures, a comparison of the raised IR bands in the UHV-FTIR measurements and theoretical IR computations indicates the formation of significant amounts of η^2-diolate.

■ ASSOCIATED CONTENT

Supporting Information

The Supporting Information is available free of charge on the ACS Publications website at DOI: 10.1021/acs.jpcc.8b04222.

Comparison of the energetic and vibrational properties of acetone adsorbed on rutile TiO_2(110) for various exchange-correlation functionals; computational study on the adsorption of enolate on rutile TiO_2(110) (PDF)

■ AUTHOR INFORMATION

Corresponding Authors

*E-mail: heshmat.noei@desy.de (H.N.).
*E-mail:gregor.feldbauer@tuhh.de. Phone: +49 (0)40 428783644. Fax: +49 (0)40 428782647 (G.F.).

ORCID

Andreas Stierle: 0000-0002-0303-6282
Yuemin Wang: 0000-0002-9963-5473
Heshmat Noei: 0000-0003-1294-3527
Gregor Feldbauer: 0000-0002-9327-0450

Notes

The authors declare no competing financial interest.

■ ACKNOWLEDGMENTS

The authors gratefully acknowledge financial support from the German Research Foundation (DFG) via SFB 986 "M^3", projects A4 and A7. All of the presented structures were visualized with Vesta.[64]

■ REFERENCES

(1) Petrik, N. G.; Henderson, M. A.; Kimmel, G. A. Insights into acetone photochemistry on rutile TiO_2 (110). 1. Off-normal CH_3 ejection from acetone diolate. *J. Phys. Chem. C* **2015**, *119*, 12262−12272.

(2) Henderson, M. A. A surface science perspective on TiO_2 photocatalysis. *Surf. Sci. Rep.* **2011**, *66*, 185−297.

(3) Setvin, M.; Shi, X.; Hulva, J.; Simschitz, T.; Parkinson, G. S.; Schmid, M.; Valentin, C. D.; Selloni, A.; Diebold, U. Methanol on anatase TiO_2 (101): Mechanistic insights into photocatalysis. *ACS Catal.* **2017**, *7*, 7081−7091.

(4) Guo, Q.; Zhou, C.; Ma, Z.; Ren, Z.; Fan, H.; Yang, X. Elementary photocatalytic chemistry on TiO_2 surfaces. *Chem. Soc. Rev.* **2016**, *45*, 3701−3730.

(5) Bettoni, M.; Candori, P.; Falcinelli, S.; Marmottini, F.; Meniconi, S.; Rol, C.; Sebastiani, G. V. Gas phase photocatalytic efficiency of TiO_2 powders evaluated by acetone photodegradation. *J. Photochem. Photobiol., A* **2013**, *268*, 1−6.

(6) El-Maazawi, M.; Finken, A.; Nair, A.; Grassian, V. Adsorption and photocatalytic oxidation of acetone on TiO_2: An in situ transmission FT-IR study. *J. Catal.* **2000**, *191*, 138−146.

(7) Shen, M.; Henderson, M. A. Site competition during coadsorption of acetone with methanol and water on TiO_2(110). *Langmuir* **2011**, *27*, 9430−9438.

(8) Dreyer, A.; Feld, A.; Kornowski, A.; Yilmaz, E. D.; Noei, H.; Meyer, A.; Krekeler, T.; Jiao, C.; Stierle, A.; Abetz, V.; et al. Organically linked iron oxide nanoparticle supercrystals with exceptional isotropic mechanical properties. *Nat. Mater.* **2016**, *15*, 522−528.

(9) Heckel, W.; Würger, T.; Müller, S.; Feldbauer, G. Van der Waals interaction really matters: energetics of benzoic acid on TiO_2 rutile surfaces. *J. Phys. Chem. C* **2017**, *121*, 17207−17214.

(10) Heckel, W.; Elsner, B. A. M.; Schulz, C.; Müller, S. The role of hydrogen on the adsorption behavior of carboxylic acid on TiO_2 surfaces. *J. Phys. Chem. C* **2014**, *118*, 10771−10779.

(11) Myers, R. *The 100 Most Important Chemical Compounds: A Reference Guide*; Greenwood Press: Westport, 2007.

(12) Henderson, M. A. Acetone and water on TiO_2(110): Competition for sites. *Langmuir* **2005**, *21*, 3443−3450.

(13) Xia, Y.; Zhang, B.; Ye, J.; Ge, Q.; Zhang, Z. Acetone-assisted oxygen vacancy diffusion on TiO_2 (110). *J. Phys. Chem. Lett.* **2012**, *3*, 2970−2974.

(14) Wang, Y.; Wöll, C. IR spectroscopic investigations of chemical and photochemical reactions on metal oxides: bridging the materials gap. *Chem. Soc. Rev.* **2017**, *46*, 1875−1932.

(15) Petrik, N. G.; Henderson, M. A.; Kimmel, G. A. Insights into acetone photochemistry on rutile TiO_2 (110). 2. New photodesorption channel with CH_3 ejection along the surface normal. *J. Phys. Chem. C* **2015**, *119*, 12273−12282.

(16) Diebold, U. The surface science of titanium dioxide. *Surf. Sci. Rep.* **2003**, *48*, 53−229.

(17) Pang, C. L.; Lindsay, R.; Thornton, G. Structure of clean and adsorbate-covered single-crystal rutile TiO_2 surfaces. *Chem. Rev.* **2013**, *113*, 3887−3948.

(18) Yasuo, M.-a.; Sasahara, A.; Onishi, H. Acetone adsorption on oxidized and reduced TiO_2 (110): A scanning tunneling microscope study. *J. Phys. Chem. C* **2010**, *114*, 14579−14582.

(19) Henderson, M. A. Acetone chemistry on oxidized and reduced TiO_2 (110). *J. Phys. Chem. B* **2004**, *108*, 18932−18941.

(20) Henderson, M. A. Photooxidation of acetone on TiO_2 (110): Conversion to acetate via methyl radical ejection. *J. Phys. Chem. B* **2005**, *109*, 12062−12070.

(21) Márquez, A. M.; Plata, J. J.; Sanz, J. F. Role of coverage and surface oxidation degree in the adsorption of acetone on TiO_2 (110). A density functional study. *J. Phys. Chem. C* **2009**, *113*, 19973−19980.

(22) Stodt, D.; Noei, H.; Hättig, C.; Wang, Y. A combined experimental and computational study on the adsorption and reactions of NO on rutile TiO_2. *Phys. Chem. Chem. Phys.* **2013**, *15*, 466−472.

(23) Noei, H.; Qiu, H.; Wang, Y.; Löffler, E.; Wöll, C.; Muhler, M. The identification of hydroxyl groups on ZnO nanoparticles by infrared spectroscopy. *Phys. Chem. Chem. Phys.* **2008**, *10*, 7092.

(24) Kresse, G.; Hafner, J. Ab initio molecular dynamics for liquid metals. *Phys. Rev. B* **1993**, *47*, 558.

(25) Kresse, G.; Hafner, J. Ab initio molecular-dynamics simulation of the liquid-metal-amorphous-semiconductor transition in germanium. *Phys. Rev. B* **1994**, *49*, 14251.

(26) Kresse, G.; Furthmüller, J. Efficient iterative schemes for ab initio total-energy calculations using a plane-wave basis set. *Phys. Rev. B* **1996**, *54*, 11169−11186.

(27) Kresse, G.; Furthmüller, J. Efficiency of ab-initio total energy calculations for metals and semiconductors using a plane-wave basis set. *Comput. Mater. Sci.* **1996**, *6*, 15−50.

(28) Blöchl, P. E. Projector augmented-wave method. *Phys. Rev. B* **1994**, *50*, 17953−17979.

(29) Kresse, G.; Joubert, D. From ultrasoft pseudopotentials to the projector augmented-wave method. *Phys. Rev. B* **1999**, *59*, 1758−1775.

(30) Klimeš, J.; Bowler, D. R.; Michaelides, A. Chemical accuracy for the van der Waals density functional. *J. Phys.: Condens. Matter* **2010**, *22*, No. 022201.

(31) Klimeš, J.; Bowler, D. R.; Michaelides, A. Van der Waals density functionals applied to solids. *Phys. Rev. B* **2011**, *83*, No. 195131.

(32) Román-Pérez, G.; Soler, J. M. Efficient implementation of a van der Waals density functional: Application to double-wall carbon nanotubes. *Phys. Rev. Lett.* **2009**, *103*, No. 096102.

DOI: 10.1021/acs.jpcc.8b04222
J. Phys. Chem. C 2018, 122, 19481−19490

(33) Thonhauser, T.; Cooper, V. R.; Li, S.; Puzder, A.; Hyldgaard, P.; Langreth, D. C. van der Waals density functional: Self-consistent potential and the nature of the van der Waals bond. *Phys. Rev. B* **2007**, *76*, No. 125112.
(34) Dion, M.; Rydberg, H.; Schröder, E.; Langreth, D. C.; Lundqvist, B. I. van der Waals density functional for general geometries. *Phys. Rev. Lett.* **2004**, *92*, No. 246401.
(35) Graziano, G.; Klimeš, J.; Fernandez-Alonso, F.; Michaelides, A. Improved description of soft layered materials with van der Waals density functional theory. *J. Phys.: Condens. Matter* **2012**, *24*, No. 424216.
(36) Bedolla, P. O.; Feldbauer, G.; Wolloch, M.; Gruber, C.; Eder, S. J.; Dörr, N.; Mohn, P.; Redinger, J.; Vernes, A. Density functional investigation of the adsorption of isooctane, ethanol, and acetic acid on a water-covered Fe(100) surface. *J. Phys. Chem. C* **2014**, *118*, 21428−21437.
(37) Bedolla, P. O.; Feldbauer, G.; Wolloch, M.; Eder, S. J.; Dörr, N.; Mohn, P.; Redinger, J.; Vernes, A. Effects of van der Waals interactions in the adsorption of isooctane and ethanol on Fe(100) surfaces. *J. Phys. Chem. C* **2014**, *118*, 17608−17615.
(38) Antlanger, M.; Mayr-Schmölzer, W.; Pavelec, J.; Mittendorfer, F.; Redinger, J.; Varga, P.; Diebold, U.; Schmid, M. $Pt_3Zr(0001)$: A substrate for growing well-ordered ultrathin Zirconia films by oxidation. *Phys. Rev. B* **2012**, *86*, No. 035451.
(39) Choi, J. I. J.; Mayr-Schmölzer, W.; Mittendorfer, F.; Redinger, J.; Diebold, U.; Schmid, M. The growth of ultra-thin Zirconia films on $Pd_3Zr(0001)$. *J. Phys.: Condens. Matter* **2014**, *26*, No. 225003.
(40) Carrasco, J.; Liu, W.; Michaelides, A.; Tkatchenko, A. Insight into the description of van der Waals forces for benzene adsorption on transition metal (111) surfaces. *J. Chem. Phys.* **2014**, *140*, No. 084704.
(41) Matos, J.; Yildirim, H.; Kara, A. Insight into the effect of long range interactions for the adsorption of benzene on transition metal (110) surfaces. *J. Phys. Chem. C* **2015**, *119*, 1886−1897.
(42) Mittendorfer, F.; Garhofer, A.; Redinger, J.; Klimeš, J.; Harl, J.; Kresse, G. Graphene on Ni (111): Strong interaction and weak adsorption. *Phys. Rev. B* **2011**, *84*, No. 201401.
(43) Liu, W.; Carrasco, J.; Santra, B.; Michaelides, A.; Scheffler, M.; Tkatchenko, A. Benzene adsorbed on metals: concerted effect of covalency and van der Waals bonding. *Phys. Rev. B* **2012**, *86*, No. 245405.
(44) Endlich, M.; Michl, A.; Hildisch, J.; Müller, S.; Kröger, J. Energy and spectroscopic line shape of the C-O stretch mode on Ir (111) in the presence of organic molecules. *J. Phys. Chem. C* **2016**, *120*, 11490−11497.
(45) Perdew, J. P.; Burke, K.; Ernzerhof, M. Generalized gradient approximation made simple. *Phys. Rev. Lett.* **1996**, *77*, 3865.
(46) Csonka, G. I.; Perdew, J. P.; Ruzsinszky, A.; Philipsen, P. H.; Lebègue, S.; Paier, J.; Vydrov, O. A.; Ángyán, J. G. Assessing the performance of recent density functionals for bulk solids. *Phys. Rev. B* **2009**, *79*, No. 155107.
(47) Perdew, J. P.; Wang, Y. Accurate and simple analytic representation of the electron-gas correlation energy. *Phys. Rev. B* **1992**, *45*, 13244.
(48) Monkhorst, H. J.; Pack, J. D. Special points for Brillouin-zone integrations. *Phys. Rev. B* **1976**, *13*, 5188.
(49) Blöchl, P.; Jepsen, O.; Andersen, O. Improved tetrahedron method for Brillouin-zone integrations. *Phys. Rev. B* **1994**, *49*, 16223−16233.
(50) Oviedo, J.; San, M.; Sanz, J. Oxygen vacancies on TiO_2 (110) from first principles calculations. *J. Chem. Phys.* **2004**, *121*, 7427−7433.
(51) Makov, G.; Payne, M. Periodic boundary conditions in ab initio calculations. *Phys. Rev. B* **1995**, *51*, 4014.
(52) Neugebauer, J.; Scheffler, M. Adsorbate-substrate and adsorbate-adsorbate interactions of Na and K adlayers on Al (111). *Phys. Rev. B* **1992**, *46*, 16067.
(53) Baroni, S.; Giannozzi, P.; Testa, A. Greens-function approach to linear response in solids. *Phys. Rev. Lett.* **1987**, *58*, 1861.
(54) Gonze, X. Perturbation expansion of variational principles at arbitrary order. *Phys. Rev. A* **1995**, *52*, 1086.
(55) Giannozzi, P.; Baroni, S. Vibrational and dielectric properties of C_{60} from density-functional perturbation theory. *J. Chem. Phys.* **1994**, *100*, 8537−8539.
(56) Giannozzi, P.; Baroni, S. In *Handbook of Materials Modeling*; Yip, S., Ed.; Springer Netherlands: Dordrecht, 2005; pp 195−214.
(57) Karhánek, D.; Bučko, T.; Hafner, J. A density functional study of the adsorption of methane-thiol on the (111) surfaces of the Ni-group metals: I. Molecular and dissociative adsorption. *J. Phys.: Condens. Matter* **2010**, *22*, No. 265005.
(58) Porezag, D.; Pederson, M. R. Infrared intensities and Raman-scattering activities within density-functional theory. *Phys. Rev. B* **1996**, *54*, 7830−7836.
(59) Alecu, I. M.; Zheng, J.; Zhao, Y.; Truhlar, D. G. Computational thermochemistry: Scale factor databases and scale factors for vibrational frequencies obtained from electronic model chemistries. *J. Chem. Theory Comput.* **2010**, *6*, 2872−2887.
(60) Skibinski, E. S.; DeBenedetti, W. J. I.; Hines, M. A. Solution deposition of phenylphosphinic acid leads to highly ordered, covalently bound monolayers on TiO_2 (110) without annealing. *J. Phys. Chem. C* **2017**, *121*, 14213−14221.
(61) Li, X.; Paier, J. Adsorption of water on the Fe_3O_4 (111) surface: Structures, stabilities, and vibrational properties studied by density functional theory. *J. Phys. Chem. C* **2016**, *120*, 1056−1065.
(62) Li, X.; Paier, J.; Sauer, J.; Mirabella, F.; Zaki, E.; Ivars-Barceló, F.; Shaikhutdinov, S.; Freund, H.-J. Surface termination of Fe_3O_4 (111) films studied by CO adsorption revisited. *J. Phys. Chem. B* **2018**, *122*, 527−533.
(63) Shimanouchi, T. In *NIST Chemistry WebBook*; Linstrom, P., Mallard, W., Eds.; NIST Standard Reference Database Number 69; National Institute of Standards and Technology: Gaithersburg, 2016.
(64) Momma, K.; Izumi, F. VESTA 3 for three-dimensional visualization of crystal, volumetric and morphology data. *J. Appl. Crystallogr.* **2011**, *44*, 1272−1276.

DOI: 10.1021/acs.jpcc.8b04222
J. Phys. Chem. C 2018, 122, 19481−19490